Unprecedented Platinum(II) Coordination compound of Sterically Hindered 3,3'-bis(NH-benzimidazol-2-yl)-2,2'-bipyridine Ligand

Zekeriya Doğan[1], Nursel Açar Selçuki[2], Simon J. Coles[3], Abdurrahman Şengül[4]

[1] Department of Civil Engineering, Faculty of Engineering, Zonguldak Bülent Ecevit University, 67100 Turkey.
E-mail: zekeriyadogan@hotmail.com Tel: +90 505 266 38 08 ORCID No: 0000-0002-2721-4450
[2] Department of Chemistry, Faculty of Science, Ege University, 35100 Bornova Izmir Turkey
E-mail: nursel.acar@ege.edu.tr Tel: +90 232 311 2387 ORCID No: 0000-0001-9292-0637
[3] School of Chemistry, University of Southampton, University Road, Highfield, Southampton SO17 1BJ, England
E-mail: .J.Coles@soton.ac.uk Tel: +44 0238 059 6721 ORCID No: 0000-0001-8414-9272
[4] Department of Chemistry, Faculty of Arts and Sciences, Zonguldak Bülent Ecevit University, 67100 Zonguldak, Turkey
E-mail: sengul@beun.edu.tr; Fax: +90 372 257 4181; Tel: + 90 372 291 1126 ORCID No: 0000-0001-6851-4612

The synthesis, spectroscopic characterization, single-crystal X-ray diffraction (SCXD) analysis, and Density Functional Theory (DFT) and time-dependent DFT (TD-DFT) studies of the coordination compound of *cis*-dichloroplatinum(II) with a sterically hindered N_4-donor ligand, 3,3'-bis(NH-benzimidazol-2-yl)-2,2'-bipyridine (L), $[Pt(L)Cl_2]\cdot DMSO$ (**1**) (DMSO = dimethylsulphoxide) are reported. The Pt(II) ion adopts a slightly distorted square-planar geometry in which L coordinates in a bidentate fashion to the metal center via unprecedented way through N atom of benzimidazole (bim) and N atom of pyridine (py) to form a seven-membered ring. The molecular units in the lattice are held together in a head to tail fashion as a dimer through intermolecular hydrogen bonding between the uncoordinated bim and py rings in the molecule through N–H···N hydrogen bonds with the R_2^2 (14) graph-set motif. The lattice DMSO solvent molecule significantly stabilizes the structure through N–H···O hydrogen bond with the coordinated bim in the structure. Hirshfeld surface analysis also confirmed the hydrogen bond interactions in the crystal. DFT and TD-DFT results show that optimized geometry and UV-vis absorption spectra are consistent with the experimental results. Natural

bond orbital (NBO) properties show that the hydrogen bond stability between two monomers is attributed to large stabilization energy values.

KEYWORDS Platinum, bipyridine, benzimidazole, X-ray, H-bond, DFT

1 INTRODUCTION

The coordination compounds of sterically hindered ligand, 3,3'-bis(NH-benzimidazol-2-yl)-2,2'-bipyridine, exhibit luminescence properties at room temperature [1–4]. The ligand incorporating pyridine and benzimidazole moieties functions as a hydrogen donor and acceptor. Therefore, it is of interest in supramolecular chemistry due to non-covalent interactions that play a significant role in the formation and stabilization of the structures [4]. The previous studies on the transition metal complexes of this ligand reveal that the ligand coordinates to the metal center solely through the benzimidazole N atoms in a bidentate fashion [1–4]. The ligand forms 1:1 complexes with Co(II) and Cu(II), and 1:2 complex with Zn(II) ion [2]. In all complexes, the metal center preferentially adopts a distorted tetrahedral geometry. The dihedral angles between the pyridine and benzimidazole rings depend on the hydrogen bonding ability of the ligand (intramolecular N–H···N bonds) [4]. The binding of the ligand to the metal center usually increases the intensity of the emission maxima and also causes a blue shift due to coordination which influences the conjugation in the molecule [1]. These spectral changes brought by the solvent molecules are of significance to the development of chemical sensors [5]. These compounds show luminescence changes in the visible spectral region upon coordination to the metal ion and also upon changing the pH of the solution [2]. The metal center in the coordination compounds of the ligand with Cu(II), Co(II), Zn(II), Cu(I), and Ag(I) ions shows a preference for a distorted tetrahedral geometry [2]. To the best of our knowledge, this is the first study on the coordination chemistry of the ligand with a d^8 platinum(II) ion. It is well known that the diamine-platinum(II) complexes show intriguing spectroscopic properties due to Pt···Pt stacking interactions in the solid-state lattice [6]. Motivated by this synergy and its potential supramolecular properties, here we report the synthesis, single-crystal X-ray analysis, spectroscopic properties, Hirshfeld Surface (HS) analysis, DFT studies, and

electronic properties of the platinum(II) complex with this very interesting sterically encumbered ligand having hydrogen donor and acceptor ability.

2 EXPERIMENTAL

2.1 Materials and instrumentation

All analytical grade reagents were obtained from commercial sources and used without further purification unless otherwise stated. Infrared spectra were recorded on a Perkin-Elmer Spectrum 100 FT-IR spectrophotometer with an attenuated total reflection (ATR) accessory featuring a zinc selenide (ZnSe) crystal at room temperature. Electronic absorption spectra were measured on a CARY 100 Bio UV-Visible spectrophotometer in DMSO solution at room temperature. The ^{1}H NMR spectra were obtained at room temperature in DMSO-d_6 using an Agilent 300 MHz Premium Compact NMR spectrometer. Chemical shifts are given in parts per million with reference to TMS. MS analyses were performed by using Agilent 6530 Accurate-Mass Quadrupole Time-of-Flight LC/MS. The ligand, 3,3'-bis(NH-benzimidazole)-2,2'-bipyridine (L) was prepared as previously reported by us [2]. Characterization data for L are identical to those of the reported data [2].

2.1 Synthesis of dichloro-(3,3'-bis(NH-benzimidazol-2-yl)-2,2'-bipyridine)platinum(II) dimethylsulphoxide (1)

The preparation of $[Pt(L)Cl_2]\cdot(CH_3)_2SO$ (**1**) was adapted from the literature method [7]. To the solution of K_2PtCl_4 (0.41 g; 1.0 mmol) in hot water (50 cm^3) was added L (0.43g; 1.10 mmol) in HCl (3M, 15 mL) at rt, The reaction mixture was set to reflux for 12 h with vigorous stirring. The precipitate as yellow solid was filtered and washed with water and ethanol. The single crystals of good quality for X-ray diffraction analysis were obtained by slow diffusion of diethyl ether into a concentrated DMSO solution at r.t. FT-IR (KBr, ν cm^{-1}); 3576 (m, νOH), 3393 (w,

νN-H), 3156 (m, νAr-H), 3065 (νAr-H), 1616 (w, δOH), 1590 (w, δN-H), 1561 (s, py and bim rings), 1520 (s, py and bim rings) , 1485 (s, py and bim rings), 1465 (s, py and bim rings), 1446 (s), 1400 (m), 1259 (w), 1161 (m), 1104 (m), 1027 (m), 816 (m), 774(vs, δAr-H) , 763 (vs, δAr-H), 707 (vs, δAr-H). LC-ESI-MS m/z: 647.1. ^{1}H NMR (300 MHz, DMSO-d_6): δ 8.5 (d, J = 7.8 Hz, 2H, 6,6′-bpy), 8.4 (d, J = 4.8 Hz, 2H, 4,4′-bpy), 8.1 (d, J = 7.9 Hz, 2H, 5,5′-bpy), 7.8 (d, J = 7.8 Hz, 2H, benzene ring), 7.7–7.6 (m, 6H, benzene ring).

2.2 Crystal structure determination

Data collections were performed on a Bruker-Nonius KappaCCD diffractometer equipped with a rotating anode to produce graphite-monochromatic Mo-K_α radiation. The structure was solved by direct methods using SHELXT [8] and refined by full-matrix least-squares methods on F^2 using SHELXL [8] from within the Olex2 [9] suite of software. The H atoms of C atoms were refined using the riding model. Molecular diagrams were created using Olex2 and Mercury [10]. Details of data collections and crystal structure determinations are gathered in Table 1. The selected bond lengths and angles for **1** are listed in Table S1 and S2, respectively. The hydrogen-bonds geometries are summarized in Table 2. Crystallographic data for the structures reported in this paper have been deposited in the Cambridge Crystallographic Data Center with CCDC deposition number 1010892 and RefCode XONLOD for **1**.

"Table 1"

Hirshfeld Surface (HS) analysis [11] for the crystal structure of **1** was carried out with Crystal Explorer version3.1 [12] to clarify the formation of the dimer structure by H-bond interaction.

2.3. Computational details

The geometry optimizations were performed with Gaussian09 [13] using Density functional theory (DFT) [14–16] with the ωB97XD functional [17] in combination with

6-31G(d,p) and LANL2DZ [18] basis sets. This functional was chosen as it has long-range terms and can calculate weak dispersion interactions [17]. Gaussview5.0 [19] was used for visualization. The minimum nature of all optimized structures was verified with frequency calculations at the same level. The time-dependent DFT (TD-DFT) calculations were performed to calculate the UV-vis absorption spectra (n = 80 states) and molecular orbital energies using the ground-state optimized geometries. TD-DFT calculations were performed with Becke's 3 parameter exchange and Lee-Yang-Parr correlation functionals (B3LYP) [20] and were repeated with CAM-B3LYP (Coulomb-Attenuating Method) [21] and ωB97XD functionals in combination with 6-31G(d,p) and LANL2DZ basis sets to obtain UV-vis spectra and both computational results were compared with experimental UV-vis absorption spectra. To mimic the real systems, all calculations were done in solution. Polarizable Continuum Model (PCM) [22] was used in all DFT and TD-DFT calculations to investigate solvent effects on the electronic transitions in solution.

The natural bonding orbitals (NBO) calculations were performed using NBO 3.1 program [23] as implemented in Gaussian 09 package. The second-order Fock matrix was used to evaluate the donor-acceptor interactions on the NBO basis.

3 RESULTS AND DISCUSSION

3.1 Synthesis and Characterization

The synthesis of **1** is illustrated in Scheme 1.

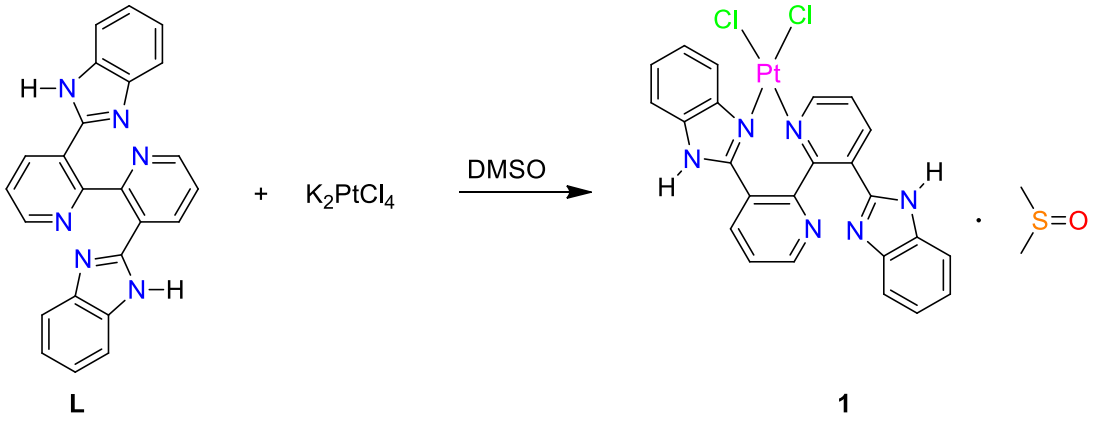

L 1

Scheme 1

The ESI-MS spectrum (Fig.S1) of **1** shows the mono cationic peak at *m/z* 619.0 $[Pt(L)+Cl]^+$ ($C_{24}H_{16}N_6PtCl$). The major peak at *m/z* 697.1 is attributed to $[Pt(L)+Cl+(CH_3)_2SO)]^+$ ($C_{26}H_{22}N_6SOPtCl$) which confirms the solvated of the ion in solution as revealed by the X-ray analysis. The ^1H NMR spectrum of **1** is shown in Fig. S2. The most striking feature of the spectrum is that due to C_2 symmetry in solution, only one set of signals assigned to the two halves of the 2,2′-bipyridine unit is observed. This is confirmed by the integration of the protons since the number of protons present in the spectrum is well-matched with the stoichiometry of **1**. The ^1H NMR spectrum is very much similar to those of the copper(I) and silver(I) complexes of the ligand [2]. In the present spectrum, the signal corresponding to the N-H proton is missing due to exchange with the deuterated solvent which resonates at 3.85 ppm for HOD. The comparison with the free ligand [1] indicates that the signals corresponding to the py protons in **1** undergo deshielding (the signals for the py protons in L appear at 8.47 as a doublet, 8.33 as a doublet, and 7.56 as a quartet). The signals for the py protons in the NMR spectrum of the zinc(II)-*bis*-complex [1] appear at 8.5 ppm as a quartet, 7.8 ppm as a triplet, and 7.7 ppm as a doublet, respectively. It is clear that upon coordination to the metal center, substantial changes relative to the free ligand are observed. The most pronounced deshielding is observed in the spectrum of **1** compared with those of the Zn(II) [21], and Cu(I) and Ag(I)-*bis*-complexes [2].

The signals corresponding to the benzene protons in the present structure also show deshielding in comparison to those of the free ligand and Zn(II) [1], and Cu(I), and Ag(I) complexes. One should bear in mind that L in the *bis*-complexes, such as Zn(II), Cu(I), and Ag(I) [2], coordinates to the metal center through only the bim N atoms, and the py N atoms remain as uncoordinated [2]. The significant deshielding of the py protons in the present spectrum of **1** may be ascribed to the coordination of the py N atom to the Pt(II) center as revealed by the X-ray analysis (vide infra).

The IR spectrum of **1** is shown in Fig. S3, The N-H stretch appears at 3576 cm^{-1}, which is consistent with that reported for benzimidazole [24]. The weak band at 3312 cm^{-1} is assigned to the OH stretching of the bound water molecule [24]. The parental absorption is observed at the lower frequency at 1616 cm^{-1} may be assigned to the bending vibration of the OH, as well. The band at 3156 cm^{-1} may be assigned to the N-H bending vibration [25], while the band at 3065 cm^{-1} is readily assigned to the aromatic C-H stretching vibration. The py and bim ring stretching vibrations appear in the region of 1590-1520 cm^{-1}. The out-of-plane bending modes for the py and bim rings are observed below 1485 cm^{-1}, and those related to bending modes of the Ar-H appear in the region of 816-707 cm^{-1}.

The UV-vis absorption and emission spectra of **1** in DMSO are depicted in Fig. 1. In the UV spectrum, the high-intense absorption bands at $\lambda \approx 283$ nm are assignable to the intraligand $\pi \rightarrow \pi^*$ transitions of the free ligand [26]. The relatively low-energy absorptions bands originating from metal-to-ligand charge-transfer (MLCT) transitions may lie underneath the broad absorbance as suggested for the related platinum(II) complexes [6,26]. Fig. 1 also depicts the emission spectra of **1** with the emission maxima at 450 nm. The emission is similar to the free ligand [2] and the related coordination compounds [1]. The emission intensity increases upon coordination to the metal ion as observed for the related cases [1,2]. The enhanced luminescence was attributed to the rigidity of the coordinated ligand which reduces the

nonradiative decay in the excited state [1]. As revealed by the X-ray analysis, the compound forms adduct with DMSO in the solid-state (vide infra). The emission band at about 450 nm is assignable to the intraligand charge-transfer (ILCT) transitions since similar emission bands are observed for the analogous Zn(II)-*bis*-complex [1] and also for Ag(I) and Cu(I) complexes [2].

"Fig. 1"

3.2. Structure description of 1

The crystal structure of **1** is shown in Fig. 2. The experimental and calculated bond lengths and angles are listed in Table S1 and S2, respectively. The hydrogen bonding parameters are given in Table 2. The SCXD analysis reveals a discrete mononuclear neutral complex, **1**, which consists of L acting as a bidentate ligand through the N atom of the py and bim rings and two Cl atoms, and an adduct of DMSO. This new complex features very interesting coordination modes. The transition metal complexes of the ligand with Cu(II) [4], Zn(II) [1], Ag(I), and Cu(I) [2] have been published. The ligand in all these complexes invariably acts as a bidentate *bis*(imidazole) donor ligand coordinating to the metal center solely through the N atoms of the bim rings, whereas the py N atoms remain uncoordinated. The present study reports the unprecedented coordination compound of the ligand with a Pt(II) ion. In the present structure, the ligand acts in a bidentate fashion and binds to the metal center via both the py and bim rings as depicted in Fig. 3. The Pt atom adopts a distorted square-planar coordination environment with two N atoms from the ligand (one N atom from py2 and one N atom from bim1 forming a seven-membered ring) and two chlorine atoms to form a *cis*-PtN_2Cl_2 chromophore as depicted in Fig. 3. Pt1 is in near ideal square planar geometry, with the mean deviation from the plane defined by Pt1 and its coordinated atoms being 0.002(1) Å. The angles of N(4)–Pt(1)–Cl(2) 177.76(8)° and N(1)–Pt(1)–Cl(1) 177.99(8)° indicate a very small degree of distortion, while

the N1–Pt1–N4 87.96(11)° and Cl1–Pt1–Cl2 91.53(3)° bite angles are also very close to the ideal for a perfect square-planar geometry. These angles are consistent with the analogous metal complexes of the py-bim ligands [27–29]. The Pt–N1 (bim) distance of 2.016(3) Å is slightly shorter than Pt–N4 (py) 2.023(3) Å, as found in other platinum(II)-pyridyl-benzimidazole complexes [4]. The slight difference in the Pt–Cl bond lengths, Pt–Cl1 2.3032(8) Å and Pt–Cl2 2.3009(8) Å, reflects the *trans*-effect of the imidazole chromophore, which is more basic than pyridine and thus more strongly coordinates to the metal center. The free ligand in the solid-state adopts a *trans*-conformation with two bim fragments on the opposite sides of the 2,2′-bipyridine backbone [4], with py-py and bim-bim dihedral angles reported as 72.5° and 99.3°, respectively. The large angles are accounted for the intramolecular N–H···N hydrogen bonds [4]. In **1**, the plane of the py rings are inclined at 60.36°, whereas the py and bim rings are inclined at 40.06° and 45.89° respectively. These dihedral angles are dramatically different to those observed for the related distorted tetrahedral complexes [2]. The smaller dihedral angles in **1** are obviously due to the coordination of the bim and py rings residing on the different halves of the molecule. This coordination mode of the ligand makes it possible to accommodate a square-planar complex. The binding of the ligand to the Pt atom forms a seven-membered ring. The molecular structure of **1** is stabilized by intermolecular complementary hydrogen bonds between the py and bim rings ($N–H_{(bim)}\cdots N_{(py)}$) in the neighboring molecules as illustrated in Fig. 4. The uncoordinated benzimidazole group forms an intramolecular hydrogen bond with the DMSO molecule through $N–H_{(bim)}\cdots O$ (Table 2). The molecular units in the lattice are held together in a head to tail fashion as a dimer through N–H···N hydrogen bonds with the R_2^2 (14) graph-set motif.

"Fig. 2"

"Table 2"

"Fig. 3"

"Fig. 4"

HS analysis indicates several intermolecular interaction sites within the crystalline structure. The surfaces plotting d_{norm} (normalized contact distance) illustrate interactions represented by different colors; red spots indicate close contacts (generally covalent nature intermolecular interactions), while white and blue colors are used for intermediate and weak interactions between the neighboring molecules. Fig. 5 shows Hirshfeld surfaces of the monomer plotted over d_{norm} in the range of -0.7499 to 1.6737 a.u. and hydrogen bonds with the adjacent molecule. Strong interactions (red spots) are in the region of the N of pyridine and bim in the whole molecule illustrating that the dimer is linked through H-bonding of N atoms.

"Fig. 5"

The normalized contact distance based on d_e (distance from the Hirshfeld surface to the nearest nucleus outside the surface), d_i (distance to the nearest nucleus inside the surface), and the van der Waals radius of the atom are shown. In d_e and d_i, the shortest, intermediate, and long distances are denoted by red, green, and blue colors respectively (Fig. S4).

A shape index in the range of -1 to 1 a.u. for the compound shows triangular red regions around the rings, indicating the presence of stacking interactions. Curvedness mapping for the compound has regular green sections indicating the presence of parallel stacking interactions (Fig. S4).

3.3. DFT studies

The optimized geometries of the most stable structures for **1** as a monomer and dimer are shown in Fig. 6. The monomers are interconnected with each other by intermolecular H-bonds to form

a dimer with a helical shape. The experimental and the calculated bond distances and angles are listed in Table S1 and Table S2 respectively for comparison. Fig. S5 provides a better understanding of all the differences in the distances and Table 3 shows the selected bond lengths [Å] and angles (°) for the monomer and dimer for comparison calculated using ωB97XD functional with 6-31G(d,p) and LANL2DZ (for Pt) basis sets.

"Fig. 6"

The experimental and calculated bond distances are generally similar for the monomer molecule. The small deviations in the calculated data from the experimental XRD data may be due to the solvent effects in the optimized structure. Additionally, while the calculations are carried out for a single molecule in DMSO using an implicit solvent model, the experimental measurements are in the solid-state with the presence of neighboring molecules.

Bond distances in the dimer are slightly different than those of the initial monomer. However, the N-H distances are slightly larger in the dimer structure compared to the crystal structure and the calculated monomer (1.008 Å in the monomer, 1.029 Å in the dimer, N(6)–H(6N); from 1.009 Å to 1.047 Å in the dimer N(2)–H(2N) in Table 3).

The H-bonding of the monomer with the neighboring molecule lengthens the N-H bond distance in the monomer. Hydrogen bonds are observed between N-H···N in the dimer and N-H···O with the adjacent DMSO molecule (H(6N) in bim2…N(3)' in py1', N(3) in py1….H(6N)' in bim2', H(2N) in bim1…O(1), and H(2N)' in bim1'…O(1)'). Intermolecular H-bonding interactions stabilize the framework structure.

Changes in the bond and torsion angles between the monomer and dimer are also observed. The Pt atom preserves its square planer structure. The Pt center is not coplanar with its neighboring pyridines (py1 and py2) and benzimidazole (bim1). There are small differences in the bond

angles between the monomer and dimer. For example, the N(1)–Pt(1)–N(4) angle of 87.92° in the monomer is found to be 85.12° in the dimer. Significant changes are observed in the dihedral angles. While the dihedral angle between py1 and py2 is 59.55° in the monomer structure, it is 65.03° in the dimer structure. It can be said that due to the interaction between the molecules in the dimer structure, more deviation from the plane is observed. The dihedral angle between py1 and bim1 remains approximately the same. The torsion angle between py2 and bim2 decreases from 44.95° to 29.71° and approaches a planar geometry.

"Table 3"

Table S3 shows the dipole moments (μ, in Debye), the sum of total electronic energies and zero-point energies (E+ZPE), the sum of electronic energy and thermal Free Energy Correction (E+ΔG) and stabilization energies at zero Kelvin (ΔE) and room temperature (ΔΔG) for ground-state geometries in water for **1** and the dimer. Considering the energy values related to the stability of the dimer structure, it has been observed that the dimer structure is more stable (negative ΔE and ΔΔG values). Besides the dimer structure being more polar than the monomer structure, both monomer and dimer have a high dipole moment.

Additionally, the NBO charge distribution for **1** and the dimer structures have been carried out by DFT levels (Table S4) to understand the changes in charge distribution of the systems upon H-bond formation of the molecules. It can be seen from the charge layout of the monomer and dimer molecule that N atoms (N6 or N55 in Fig. S6) participating in the H-bond in the dimer structure have increased their electron donor properties (charges for N6 in the monomer -0.461, in the dimer -0.499). It clear that the N atoms have more donor electron ability in the dimer form than that of the monomer (Fig. S7).

NBO analysis was also used to probe hydrogen bonding, the hyper conjugative interactions responsible for the compound stability and charge transmission between the electron donor (i) and acceptor (j) by Fock matrix analysis. For the dimer molecule LP(N)→σ*(N-H) and LP(O)→σ*(N-H) were observed with promising stabilization energies as presented in Table S5 and Fig. S8 (LP: lone pair electrons).

The molecular electrostatic potential (MEP) map is useful to find the suitable regions for electrophilic and nucleophilic attacks on the molecule. The total electron density was calculated using the NBO charge distribution. Fig. S9 shows the MEP of the dimer in DMSO mapped in the range between -0.126 a.u. and +0.126 a.u. Red colors of the electrostatic potentials refer to more electron density which could be favorable positions for electrophilic attacks. The negative charges are mostly localized on the electronegative Cl, O, and N atoms. C and H atoms with blue and green colors exhibiting mostly positively charged regions (electron-deficient zones). Therefore, it is more susceptible to nucleophilic attacks by other species.

Fig. S10 shows the differences of UV-Vis absorption spectra between the calculated spectra with different functionals (B3LYP, CAM-B3LYP, and ωB97XD) and the experimental one. CAM-B3LYP results are used in the discussion since they are more consistent with the experimental spectra. Fig. 7 shows the calculated and experimental UV-vis absorption spectra for the dimer in DMSO. The selected electronic transitions and the corresponding orbitals for the compound are displayed in Table S6 and Fig. S11, respectively.

"Fig. 7"

There are d-d transitions, π–π*, n–π* charge transfer (CT) transitions, metal-to-ligand charge transfer (MLCT), and ligand-to-metal charge transfer (LMCT) types upon excitation for the dimer. The maximum peak at 293.1 nm displays a π–π* intra-ligand transition from HOMO of

bim2 to LUMO+3 of py2 rings (CT1). At wavelengths between 335 nm and 386 nm, forbidden d-d transitions can be seen with weak oscillator strengths. Due to the very small intensity of the peaks, they could not be observed in the experimental spectrum. The chlorine atoms are also excited, with d orbitals in the same region. Again, in this region, at 358.3 nm, LMCT occurs from bim to Pt. MLCT from the Pt to the py and bim rings is observed at 250 nm. In general, the electronic transitions correspond to the transitions between bim and py between 250 and 300 nm. The locally excited state of benzimidazole (LE3) is observed with MLCT at 264.5 nm.

4 CONCLUSION

The research on the synthesis and characterization of the new coordination compound of platinum(II) with a sterically hindered ligand, 3,3′-bis(NH-benzimidazol-2-yl)-2,2′-bipyridine has resulted in unprecedented *cis*-[Pt(L)Cl_2]·DMSO. To the best of our knowledge, it is the first compound where this ligand coordinates to the metal center in a *cis*-disposition through both the pyridine and benzimidazole N atoms to afford a square-planar $PtCl_2N_2$ complex. The compound is solvated in the solid-state [Pt(L)Cl_2]·DMSO. The molecular units are interconnected with each other in a head to tail fashion through the complementary N–H···N hydrogen bonds with a R_2^2 (14) graph-set motif. The molecular structure is further stabilized by intermolecular N–H···O hydrogen bonding with the solvent molecule. The compound exhibits blue luminescence in solution. DFT optimized structure and the crystal structure of the monomer are consistent with each other. Hirshfeld surface analysis and NBO analysis show that the dimer structure is stabilized by H-bond formation. Electronic energy calculations and Gibbs free energy calculations confirm the stable dimer formation.

Supporting Information

The supplementary crystallographic data, CCDC Deposition Number 1010892, for (**1**) can be obtained free of charge via http://www.ccdc.cam.ac.uk/conts/retrieving.html (or from the Cambridge Crystallographic Data Centre, 12, Union Road, Cambridge CB2 1EZ, UK; fax: +44 1223 336033). Computational results are also given as supporting information.

ACKNOWLEDGEMENTS

This work was supported by the Turkish Scientific and Technological Council, Project No: TBAG-2450 (104T060). The authors are grateful to the TUBITAK-ULAKBIM Truba Resources and Fen Cluster by Ege University, Faculty of Science for computer time.

REFERENCES

[1] S. Bin Miao, B.M. Ji, C.X. Du, Synthesis and crystal structure of 3,3′-bis(2-benzimidazolyl)-2, 2′-dipyridine with hydrated zinc(II) perchlorate, Jiegou Huaxue. 26 (2007) 439–444.

[2] A. Şengül, Ö. Kurt, P.D.F. Adler, S.J. Coles, Spectroscopic and structural properties of complexes of 3,3′-bis(2-benzimidazolyl)-2,2′-bipyridine with copper(i) and silver(i), J. Coord. Chem. 67 (2014) 2365–2376. https://doi.org/10.1080/00958972.2014.943201.

[3] K.L. Cheng, S.C. Sheu, G.H. Lee, Y.C. Lin, Y. Wang, T.I. Ho, [6,6′-bis(benzimidazol-2-yl-,N 3)-2,2′-bipyridine]dichlorocobalt(II)-dimethylformamide (1/2), Acta Crystallogr. Sect. C Cryst. Struct. Commun. 53 (1997) 1238–1240. https://doi.org/10.1107/S0108270196015387.

[4] B.M. Ji, S. Bin Miao, D.S. Deng, C.X. Du, The C-H···Cl2Cu(II) synthon in the structural direction and assembly of supramolecular complexes with the 3,3′-bis(2-benzimidazolyl)-2,2′-dipyridine ligand and its N-substituted derivatives, Polyhedron. 28 (2009) 2611–2618. https://doi.org/10.1016/j.poly.2009.05.078.

[5] J. Ni, L.Y. Zhang, H.M. Wen, Z.N. Chen, Luminescence vapochromic properties of a platinum(II) complex with 5,5′-bis(trimethylsilylethynyl)-2,2′-bipyridine, Chem. Commun. (2009) 3801–3803. https://doi.org/10.1039/b901248f.

[6] R.H. Herber, C. Croft, M.J. Coyer, B. Bilash, S. Sahiner, Origin of Polychromism of Cis Square-Planar Platinum(II) Complexes: Comparison of Two Forms of [Pt(2,2′-bpy)(Cl)2], Inorg. Chem. 33 (1994) 2422–2426. https://doi.org/10.1021/ic00089a018.

[7] A. Sengül, R.D. Gillard, Addition of hydroxide to an isoelectronic series of bis-

diazineplatinum(II) complex ions, Transit. Met. Chem. 23 (1998) 663–666. https://doi.org/10.1023/A:1006936408391.

[8] G.M. Sheldrick, SHELXT - Integrated space-group and crystal-structure determination, Acta Crystallogr. Sect. A Found. Crystallogr. 71 (2015) 3–8. https://doi.org/10.1107/S2053273314026370.

[9] O. V. Dolomanov, L.J. Bourhis, R.J. Gildea, J.A.K. Howard, H. Puschmann, OLEX2: A complete structure solution, refinement and analysis program, J. Appl. Crystallogr. 42 (2009) 339–341. https://doi.org/10.1107/S0021889808042726.

[10] C.F. MacRae, I. Sovago, S.J. Cottrell, P.T.A. Galek, P. McCabe, E. Pidcock, M. Platings, G.P. Shields, J.S. Stevens, M. Towler, P.A. Wood, Mercury 4.0: From visualization to analysis, design and prediction, J. Appl. Crystallogr. 53 (2020) 226–235. https://doi.org/10.1107/S1600576719014092.

[11] M.A. Spackman, D. Jayatilaka, Hirshfeld surface analysis, CrystEngComm. 11 (2009) 19–32. https://doi.org/10.1039/b818330a.

[12] S.K. Wolff, D.J. Grimwood, J.J. McKinnon, M.J. Turner, D. Jayatilaka, M.A. Spackman, Crystal Explorer 3.1, (2012).

[13] M.J. Frisch, G.W. Trucks, H.B. Schlegel, G.E. Scuseria, M.A. Robb, J.R. Cheeseman, G. Scalmani, V. Barone, B. Mennucci, G.A. Petersson, H. Nakatsuji, M. Caricato, X. Li, H.P. Hratchian, A.F. Izmaylov, J. Bloino, G. Zheng, J.L. Sonnenberg, M. Hada, M. Ehara, K. Toyota, R. Fukuda, J. Hasegawa, M. Ishida, T. Nakajima, Y. Honda, O. Kitao, H. Nakai, T. Vreven, J.A. Montgomery, Jr., J.E. Peralta, F. Ogliaro, M. Bearpark, J.J. Heyd, E. Brothers, K.N. Kudin, V.N. Staroverov, R. Kobayashi, J. Normand, K. Raghavachari, A. Rendell, J.C. Burant, S.S. Iyengar, J. Tomasi, M. Cossi,

N. Rega, J.M. Millam, M. Klene, J.E. Knox, J.B. Cross, V. Bakken, C. Adamo, J. Jaramillo, R. Gomperts, R.E. Stratmann, O. Yazyev, A.J. Austin, R. Cammi, C. Pomelli, J.W. Ochterski, R.L. Martin, K. Morokuma, V.G. Zakrzewski, G.A. Voth, P. Salvador, J.J. Dannenberg, S. Dapprich, A.D. Daniels, Ö. Farkas, J.B. Foresman, J. V. Ortiz, J. Cioslowski, D.J. Fox, Gaussian 09, (2009). https://gaussian.com/glossary/g09/.

[14] A.D. Becke, Density-functional thermochemistry. III. The role of exact exchange, J. Chem. Phys. 98 (1993) 5648–5652. https://doi.org/10.1063/1.464913.

[15] A.D. Becke, Density-functional exchange-energy approximation with correct asymptotic behavior, Phys. Rev. A. 38 (1988) 3098–3100. https://doi.org/10.1103/PhysRevA.38.3098.

[16] W. Kohn, L.J. Sham, Self-consistent equations including exchange and correlation effects, Phys. Rev. 140 (1965) A1133--A1138. https://doi.org/10.1103/PhysRev.140.A1133.

[17] J. Da Chai, M. Head-Gordon, Long-range corrected hybrid density functionals with damped atom-atom dispersion corrections, Phys. Chem. Chem. Phys. 10 (2008) 6615–6620. https://doi.org/10.1039/b810189b.

[18] T.H. Dunning, P.J. Hay, Gaussian Basis Sets for Molecular Calculations BT - Methods of Electronic Structure Theory, in: H.F. Schaefer (Ed.), Springer US, Boston, MA, 1977: pp. 1–27. https://doi.org/10.1007/978-1-4757-0887-5_1.

[19] R. Dennington, T. Keith, J. Millam, GaussView 5.0.9, (2009).

[20] C. Lee, W. Yang, R.G. Parr, Development of the Colle-Salvetti correlation-energy formula into a functional of the electron density, Phys. Rev. B. 37 (1988) 785–789.

https://doi.org/10.1103/PhysRevB.37.785.

[21] T. Yanai, D.P. Tew, N.C. Handy, A new hybrid exchange-correlation functional using the Coulomb-attenuating method (CAM-B3LYP), Chem. Phys. Lett. 393 (2004) 51–57. https://doi.org/10.1016/j.cplett.2004.06.011.

[22] J. Tomasi, B. Mennucci, E. Cancès, The IEF version of the PCM solvation method: An overview of a new method addressed to study molecular solutes at the QM ab initio level, J. Mol. Struct. THEOCHEM. 464 (1999) 211–226. https://doi.org/10.1016/S0166-1280(98)00553-3.

[23] E.D. Glendening, A.E. Reed, J.E. Carpenter, F. Weinhold, NBO Version 3.1., (2003).

[24] A. Bhattacherjee, S. Wategaonkar, Conformational preferences of monohydrated clusters of imidazole derivatives revisited., Phys. Chem. Chem. Phys. 17 (2015) 20080–20092. https://doi.org/10.1039/c5cp02422f.

[25] J. Miao, Y. Nie, C. Hu, Z. Zhang, G. Li, M. Xu, G. Sun, Polymorphism in 3,4-bis(2-benzimidazolyl)pyridine: Controlled synthesis, crystal structures and photophysical properties, J. Mol. Struct. 1014 (2012) 97–101. https://doi.org/10.1016/j.molstruc.2012.01.051.

[26] K.C. Shih, R.H. Herber, Square planar platinum(II) complexes: synthesis, IR spectroscopy, and hydration equilibria of PtIIL(CN)2 (L = 4,4'-di-tert-butyl-2,2'-bipyridine), Inorg. Chem. 31 (1992) 5444–5449. https://doi.org/10.1021/ic00052a021.

[27] M.R. DeStefano, D.K. Geiger, A luminescent bis(pyridyl)-substituted benzimidazole platinum(II) complex exhibiting an intermolecular anagostic interaction, Acta Crystallogr. Sect. C Struct. Chem. 73 (2017) 697–702.

https://doi.org/10.1107/S2053229617011573.

[28] C. Mock, I. Puscasu, M.J. Rauterkus, G. Tallen, J.E.A. Wolff, B. Krebs, Novel Pt(II) anticancer agents and their Pd(II) analogues: Syntheses, crystal structures, reactions with nucleobases and cytotoxicities, Inorganica Chim. Acta. 319 (2001) 109–116. https://doi.org/10.1016/S0020-1693(01)00459-5.

[29] J.S. Casas, A. Castiñeiras, E. García-Martínez, Y. Parajó, M.L. Pérez-Parallé, A. Sánchez-González, J. Sordo, Synthesis and cytotoxicity of 2-(2′-pyridyl)benzimidazole complexes of palladium(II) and platinum(II), Zeitschrift Fur Anorg. Und Allg. Chemie. 631 (2005) 2258–2264. https://doi.org/10.1002/zaac.200570054.

Table 1. Structure solution and refinement parameters for **1**.

Empirical formula	$C_{26}H_{20}Cl_2N_6OPtS$	
Formula weight	730.53	
Temperature	120(2) K	
Wavelength	0.71073 Å	
Crystal system	Triclinic	
Space group	P-1	
Unit cell dimensions	a = 9.9136(3) Å	α= 109.7700(10)º.
	b = 12.5634(3) Å	β = 111.1540(10)º.
	c = 12.8377(3) Å	γ = 101.6710(10)º.
Volume	1303.93(6) $Å^3$	
Z	2	
Density (calculated)	1.861 Mg/m^3	
Absorption coefficient	5.698 mm^{-1}	
F(000)	708	
Crystal size	0.14 x 0.05 x 0.05 mm^3	
Theta range for data collection	3.24 to 27.50º.	
Index ranges	-12<=h<=12, -16<=k<=15, -16<=l<=16	
Reflections collected	27964	
Independent reflections	5957 [R(int) = 0.0321]	
Completeness to theta = 27.50º	99.6 %	
Absorption correction	Semi-empirical from equivalents	
Max. and min. transmission	0.7637 and 0.5026	
Refinement method	Full-matrix least-squares on F^2	
Data / restraints / parameters	5957 / 0 / 344	
Goodness-of-fit on F^2	1.068	
Final R indices [I>2sigma(I)]	R1 = 0.0255, wR2 = 0.0641	
R indices (all data)	R1 = 0.0272, wR2 = 0.0653	
Largest diff. peak and hole	1.340 and -1.753 $e.Å^{-3}$	

Table 2. Hydrogen bonding geometries in **1**

Interaction	D-H (Å)	D···A (Å)	H···A (Å)	D-H···A (°)
N2···H2N···O1 *i*	0.92(6)	1.74(7)	2.646(6)	171(6)
N6···H6N···N3 *ii*	0.85(6)	2.06(6)	2.868(5)	159(6)
C10···H10···Cl1 *iii*	0.9500	2.7200	3.609(4)	155.00
C20···H20···S1 *i*	0.9500	2.8400	3.725(5)	155.00
C25···H25C···Cl1	0.9800	2.8000	3.674(7)	149.00

Symmetry code: i x,y,1+z; ii -x,-y,1-z; iii 1-x,-y,1-z. D: Donor, A: Acceptor.

Table 3. Selected Bond lengths [Å], bond angles [º], and dihedral angles [º] for **1** and dimer calculated at ωB97XD/6-31G(d,p)/LANL2DZ (for Pt) basis sets.

Distances [Å]	Monomer	Dimer	**Angles [º]**	Monomer	Dimer
Pt(1)-N(1)	2.029	2.018	N(4)-Pt(1)-Cl(2)	177.02	175.71
Pt(1)-N(4)	2.048	2.050	N(1)-Pt(1)-Cl(1)	177.01	177.45
Pt(1)-Cl(2)	2.374	2.371	N(4)-Pt(1)-Cl(1)	90.33	92.46
Pt(1)-Cl(1)	2.377	2.384	Cl(2)-Pt(1)-Cl(1)	92.14	91.82
N(3)-C(12)	1.333	1.333	C(12)-N(3)-C(11)	118.36	118.61
N(3)-C(11)	1.334	1.336	C(18)-N(6)-C(24)	106.84	106.57
N(6)-H(6N)	1.008	1.029	C(18)-N(5)-C(19)	104.69	104.67
N(2)-H(2N)	1.009	1.047	C(1)-N(2)-H(2N)	125.013	128.93
N(6)-C(18)	1.368	1.366	**Dihedral angles [º]**		
N(6)-C(24)	1.378	1.375	C(14)-C(13)-C(12)-N(3)	59.55	65.03
H(6N)…N(3)’	-	1.885	N(2)-C(1)-C(8)-C(12)	131.87	130.34
N(3)….H(6N)’	-	1.911	N(6)-C(18)-C(14)-C(15)	44.95	29.71
H(2N)…O(1)	-	1.634	N(4)-Pt(1)-N(1)-C(1)	61.70	65.20
H(2N)’…O(1)’	-	1.609	Cl(1)-Pt(1)-N(1)-C(1)	31.16	83.60
Angles [º]			Cl(2)-Pt(1)-N(4)-C(17)	99.33	109.46
N(1)-Pt(1)-N(4)	86.94	85.12	C(13)-N(4)-Pt(1)-Cl(1)	122.78	120.47
N(1)-Pt(1)-Cl(2)	90.55	90.59	C(1)-N(1)-Pt(1)-Cl(2)	-119.00	-115.05

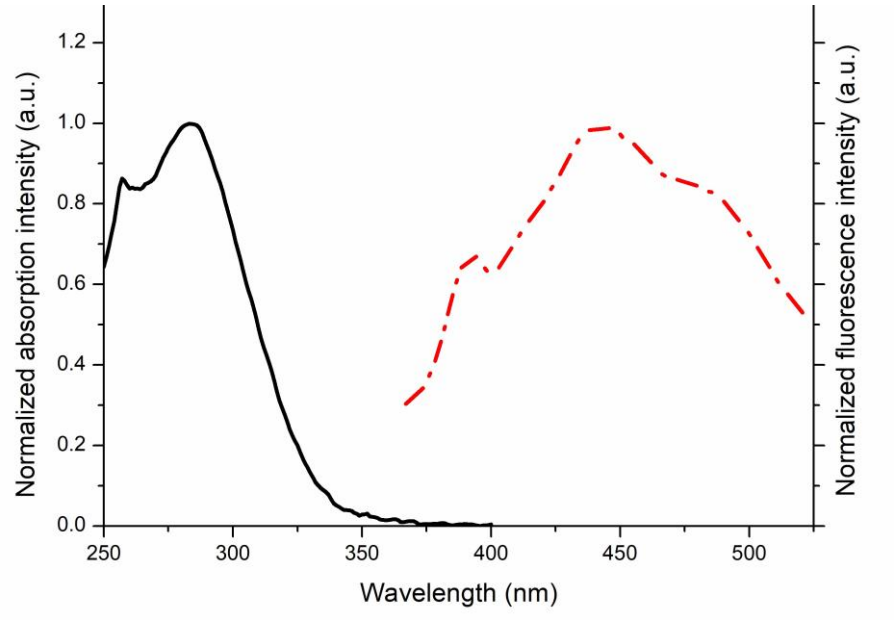

Fig. 1. Normalized UV-Vis absorption (solid line) and emission spectra of **1** in DMSO.

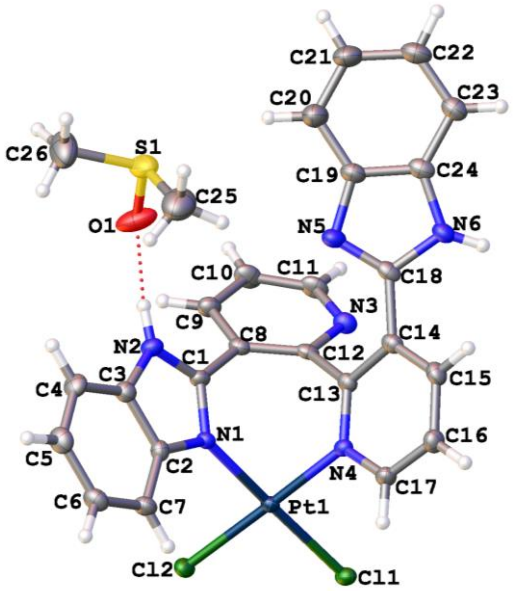

Fig. 2. Molecular structure of **1**.

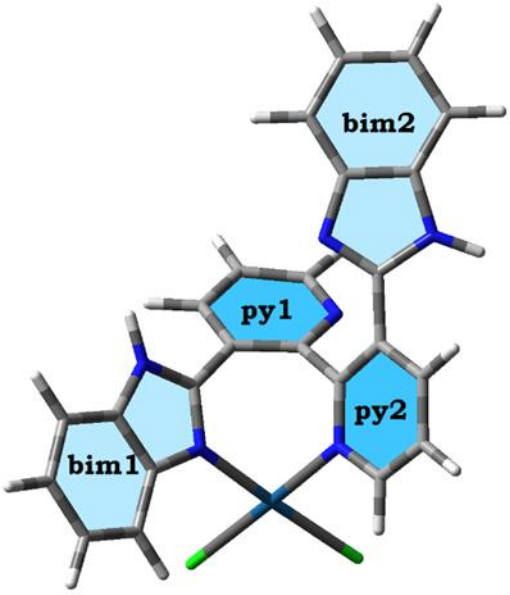

Fig. 3. The unprecedented coordination mode of the ligand.

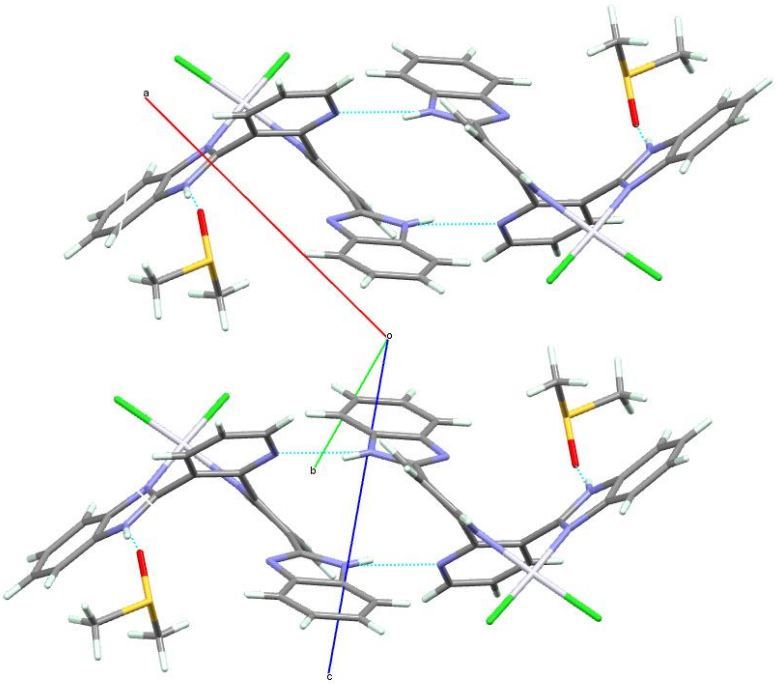

Fig. 4. The complementary hydrogen bonding and intramolecular interactions in **1**.

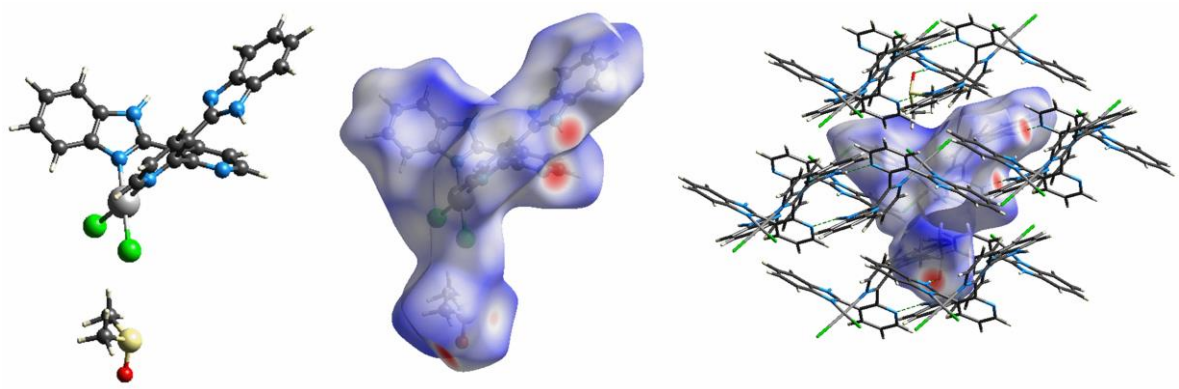

Fig. 5. Hirshfeld surface of the **1** plotted over d_{norm}

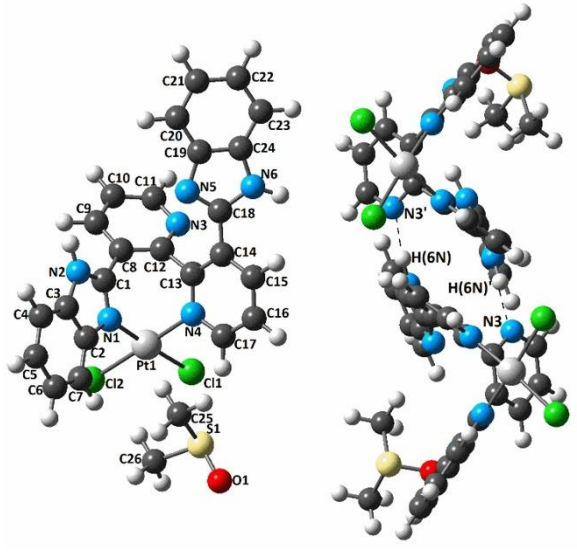

Fig. 6. Calculated **1** and dimer structure of **1** optimized in DMSO at ωB97XD functional with 6-31G(d,p) and LANL2DZ (for Pt) basis sets.

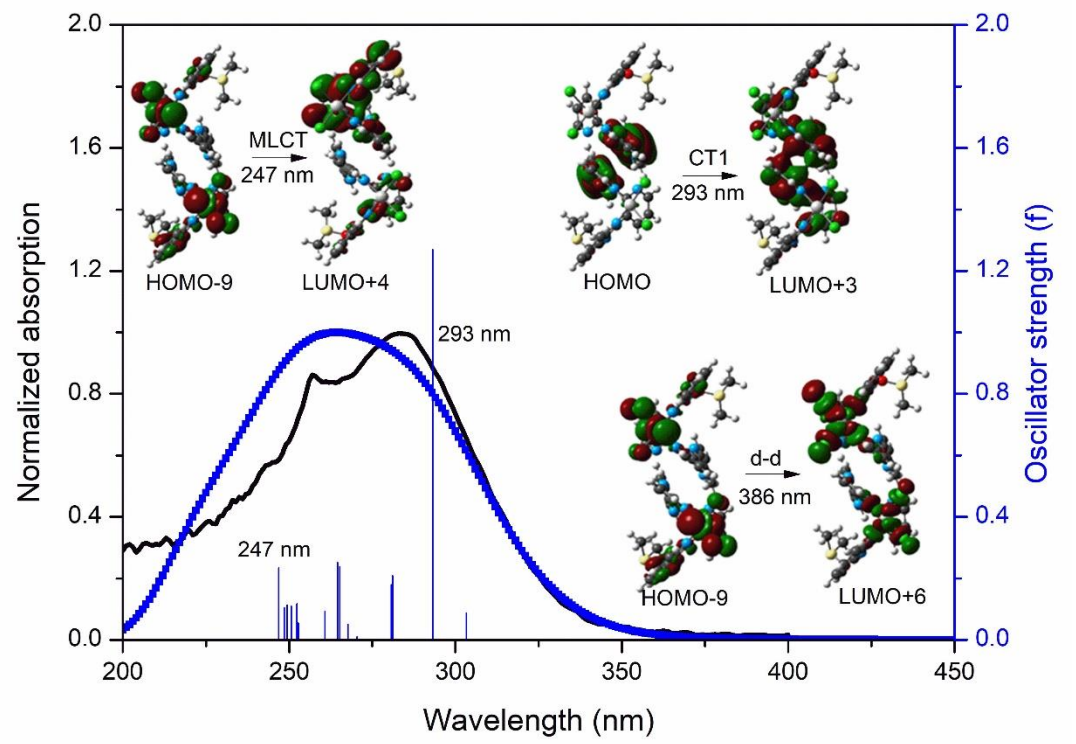

Fig. 7. The experimental (black line) and calculated (blue line) UV-vis absorption spectra of the dimer in DMSO

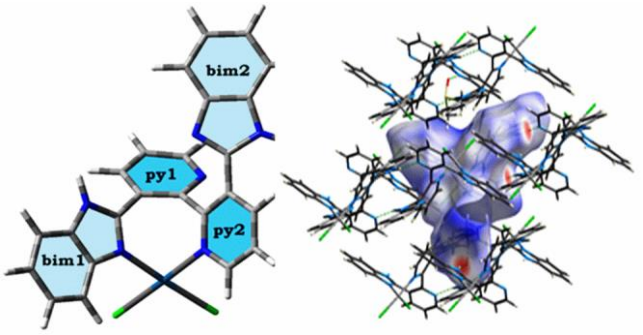
bim2
py1
py2
bim1

Supplementary Material

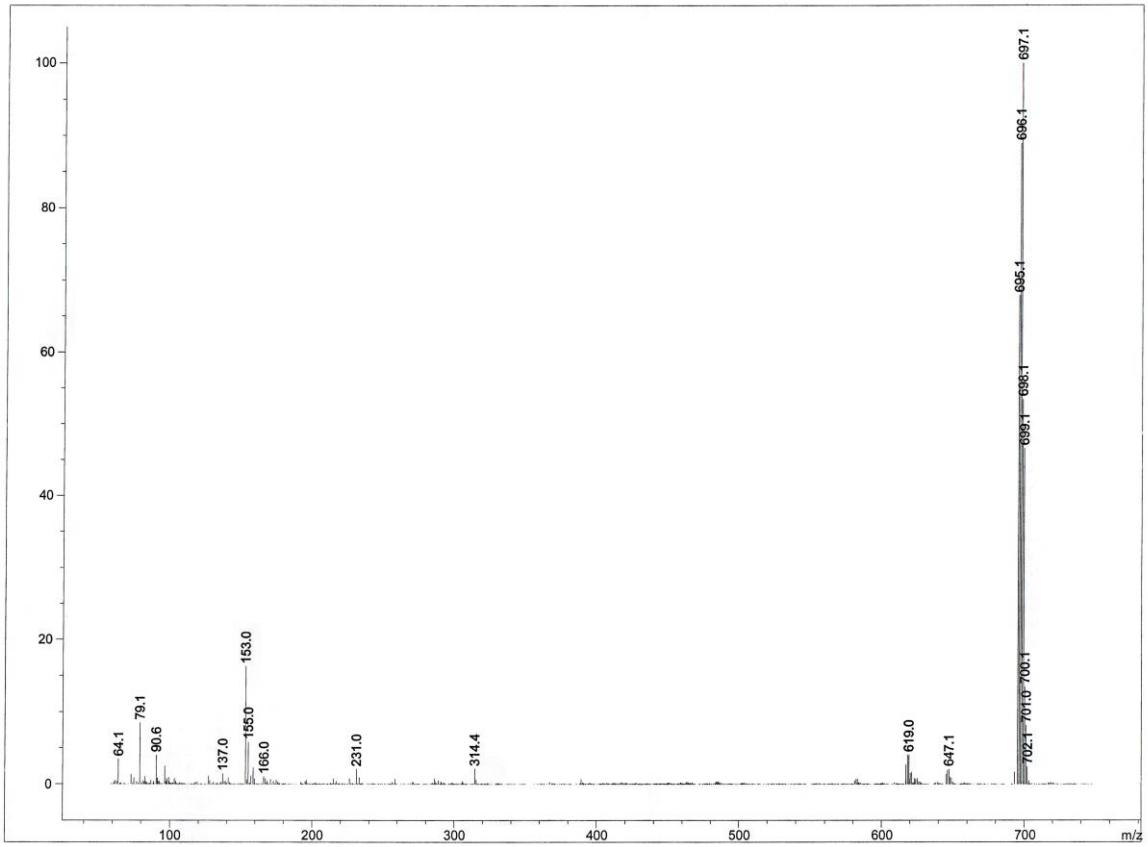

Fig. S1. ES-MS spectrum of **1**

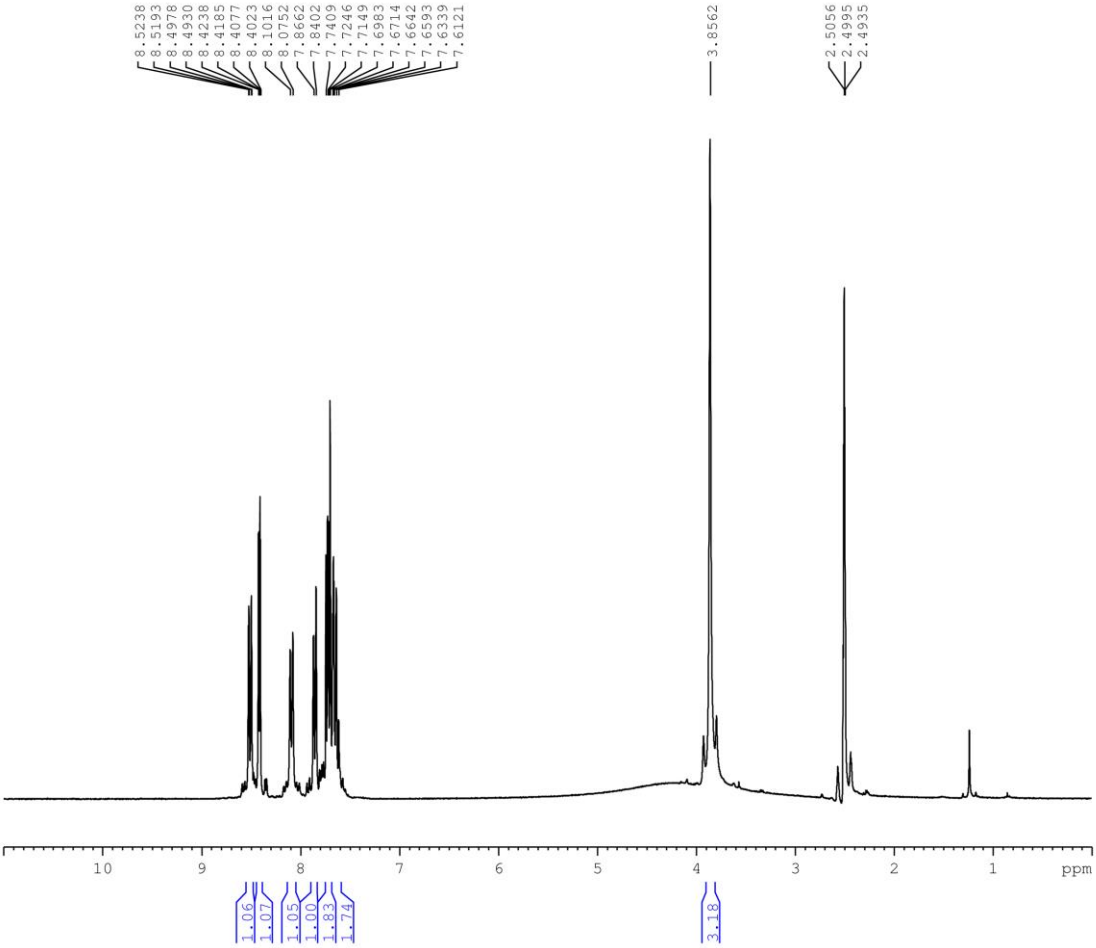

Fig. S2. ^{1}H NMR spectrum of **1**

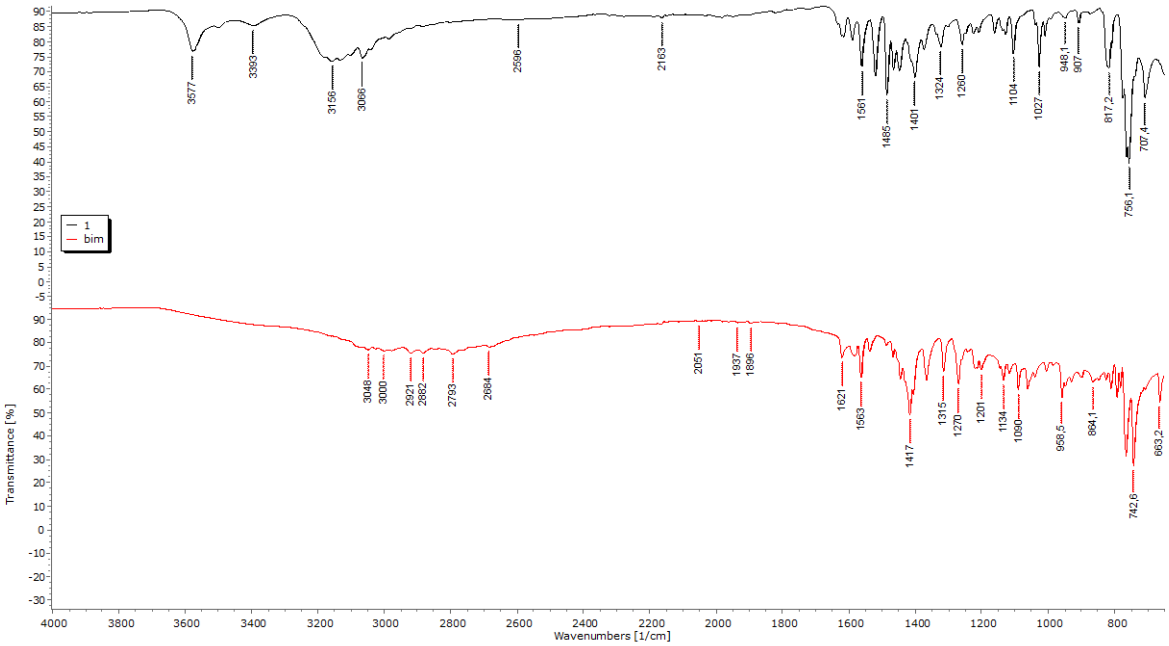

Fig. S3. FT-IR (ATR) spectrum of L and **1**

Table S1. Experimental and calculated (in DMSO) bond lengths [Å] for **1**

Distances	Exp. [Å] monomer	Calc. [Å] monomer	Calc. [Å] Dimer	Distances	Exp. [Å] monomer	Calc. [Å] monomer	Calc. [Å] Dimer
Pt(1)-N(1)	2.016(3)	2.035	2.018	C(9)-H(9)	0.9500	1.085	1.085
Pt(1)-N(4)	2.023(3)	2.054	2.050	C(10)-C(11)	1.370(6)	1.391	1.388
Pt(1)-Cl(2)	2.3009(8)	2.370	2.371	C(10)-H(10)	0.9500	1.083	1.083
Pt(1)-Cl(1)	2.3032(8)	2.374	2.384	C(11)-H(11)	0.9500	1.086	1.086
N(1)-C(1)	1.325(4)	1.325	1.329	C(12)-C(13)	1.504(5)	1.498	1.499
N(1)-C(2)	1.391(4)	1.389	1.385	C(13)-C(14)	1.404(5)	1.401	1.402
N(2)-C(1)	1.343(4)	1.349	1.343	C(14)-C(15)	1.387(5)	1.393	1.398
N(2)-C(3)	1.382(5)	1.381	1.380	C(14)-C(18)	1.479(5)	1.473	1.472
N(2)-H(2N)	0.91(6)	**1.009**	**1.047**	C(15)-C(16)	1.390(5)	1.386	1.383
N(3)-C(12)	1.345(4)	1.333	1.333	C(15)-H(15)	0.9500	1.085	1.085
N(3)-C(11)	1.351(5)	1.334	1.336	C(16)-C(17)	1.378(5)	1.381	1.384
N(4)-C(17)	1.350(4)	1.346	1.342	C(16)-H(16)	0.9500	1.082	1.084
N(4)-C(13)	1.355(4)	1.346	1.350	C(17)-H(17)	0.9500	1.082	1.082
N(5)-C(18)	1.311(5)	1.311	1.315	C(19)-C(24)	1.394(5)	1.408	1.408
N(5)-C(19)	1.390(5)	1.384	1.382	C(19)-C(20)	1.402(6)	1.400	1.403
N(6)-C(18)	1.363(5)	1.368	1.366	C(20)-C(21)	1.384(6)	1.385	1.384
N(6)-C(24)	1.383(5)	1.378	1.375	C(20)-H(20)	0.9500	1.085	1.085
N(6)-H(6N)	0.85(5)	**1.008**	**1.029**	C(21)-C(22)	1.393(7)	1.410	1.410
C(1)-C(8)	1.472(5)	1.465	1.468	C(21)-H(21)	0.9500	1.085	1.085
C(2)-C(7)	1.393(5)	1.396	1.397	C(22)-C(23)	1.377(6)	1.386	1.384
C(2)-C(3)	1.404(5)	1.402	1.401	C(22)-H(22)	0.9500	1.085	1.085
C(3)-C(4)	1.389(5)	1.395	1.396	C(23)-C(24)	1.396(5)	1.395	1.396
C(4)-C(5)	1.378(6)	1.385	1.385	C(23)-H(23)	0.9500	1.085	1.084
C(4)-H(4)	0.9500	1.084	1.084	S(1)-O(1)	1.491(4)	1.512	1.533
C(5)-C(6)	1.414(6)	1.409	1.411	S(1)-C(26)	1.772(5)	1.805	1.798
C(5)-H(5)	0.9500	1.084	1.085	S(1)-C(25)	1.802(6)	1.807	1.808
C(6)-C(7)	1.387(5)	1.384	1.385	C(25)-H(25A)	0.9800	1.091	1.092
C(6)-H(6)	0.9500	1.085	1.085	C(25)-H(25B)	0.9800	1.092	1.091
C(7)-H(7)	0.9500	1.083	1.084	C(25)-H(25C)	0.9800	1.092	1.092
C(8)-C(12)	1.393(5)	1.399	1.401	C(26)-H(26A)	0.9800	1.093	1.092
C(8)-C(9)	1.397(5)	1.394	1.393	C(26)-H(26B)	0.9800	1.093	1.090
C(9)-C(10)	1.388(5)	1.387	1.388	C(26)-H(26C)	0.9800	1.091	1.092

Table S2. Experimental and calculated (in DMSO) bond angles [º] for **1**

	Exp.	Calc.		Exp.	Calc.
N(1)-Pt(1)-N(4)	87.96(11)	87.926	C(1)-N(2)-C(3)	107.2(3)	108.279
N(1)-Pt(1)-Cl(2)	90.21(8)	90.193	C(1)-N(2)-H(2N)	124(4)	125.013
N(4)-Pt(1)-Cl(2)	177.76(8)	177.990	C(3)-N(2)-H(2N)	128(4)	126.615
N(1)-Pt(1)-Cl(1)	177.99(8)	177.466	C(12)-N(3)-C(11)	117.6(3)	118.280
N(4)-Pt(1)-Cl(1)	90.28(8)	89.892	C(17)-N(4)-C(13)	119.9(3)	119.825
Cl(2)-Pt(1)-Cl(1)	91.53(3)	92.005	C(17)-N(4)-Pt(1)	117.0(2)	117.900
C(1)-N(1)-C(2)	106.4(3)	107.134	C(13)-N(4)-Pt(1)	122.9(2)	122.143
C(1)-N(1)-Pt(1)	124.4(2)	123.333	C(18)-N(5)-C(19)	104.5(3)	104.697
C(2)-N(1)-Pt(1)	129.2(2)	129.532	C(18)-N(6)-C(24)	106.1(3)	106.835

C(18)-N(6)-H(6N)	128(4)	126.299	C(14)-C(15)-C(16)	119.5(3)	119.365
C(24)-N(6)-H(6N)	125(4)	126.555	C(14)-C(15)-H(15)	120.3	120.125
N(1)-C(1)-N(2)	112.3(3)	110.954	C(16)-C(15)-H(15)	120.3	120.505
N(1)-C(1)-C(8)	124.9(3)	124.357	C(17)-C(16)-C(15)	119.1(3)	118.739
N(2)-C(1)-C(8)	122.8(3)	124.572	C(17)-C(16)-H(16)	120.4	119.668
N(1)-C(2)-C(7)	131.2(3)	131.271	C(15)-C(16)-H(16)	120.4	121.579
N(1)-C(2)-C(3)	107.6(3)	107.965	N(4)-C(17)-C(16)	121.7(3)	122.183
C(7)-C(2)-C(3)	121.2(3)	120.757	N(4)-C(17)-H(17)	119.1	116.154
N(2)-C(3)-C(4)	131.4(3)	132.063	C(16)-C(17)-H(17)	119.1	121.661
N(2)-C(3)-C(2)	106.4(3)	105.660	N(5)-C(18)-N(6)	113.9(3)	113.414
C(4)-C(3)-C(2)	122.2(3)	122.276	N(5)-C(18)-C(14)	123.8(3)	124.809
C(5)-C(4)-C(3)	116.5(3)	116.487	N(6)-C(18)-C(14)	122.3(3)	121.755
C(5)-C(4)-H(4)	121.7	122.014	N(5)-C(19)-C(24)	110.0(3)	110.257
C(3)-C(4)-H(4)	121.7	121.499	N(5)-C(19)-C(20)	129.9(4)	129.813
C(4)-C(5)-C(6)	121.8(3)	121.649	C(24)-C(19)-C(20)	120.1(4)	119.929
C(4)-C(5)-H(5)	119.1	119.194	C(21)-C(20)-C(19)	117.5(4)	117.843
C(6)-C(5)-H(5)	119.1	119.154	C(21)-C(20)-H(20)	121.3	121.636
C(7)-C(6)-C(5)	121.5(3)	121.580	C(19)-C(20)-H(20)	121.3	120.519
C(7)-C(6)-H(6)	119.2	119.302	C(22)-C(21)-C(20)	121.5(4)	121.421
C(5)-C(6)-H(6)	119.2	119.117	C(22)-C(21)-H(21)	119.3	119.007
C(6)-C(7)-C(2)	116.7(3)	117.045	C(20)-C(21)-H(21)	119.3	119.571
C(6)-C(7)-H(7)	121.6	121.883	C(23)-C(22)-C(21)	121.9(4)	121.657
C(2)-C(7)-H(7)	121.6	120.875	C(23)-C(22)-H(22)	119.0	119.242
C(12)-C(8)-C(9)	119.0(3)	118.292	C(21)-C(22)-H(22)	119.0	119.100
C(12)-C(8)-C(1)	121.3(3)	121.595	C(22)-C(23)-C(24)	116.6(4)	116.522
C(9)-C(8)-C(1)	119.6(3)	120.083	C(22)-C(23)-H(23)	121.7	121.735
C(10)-C(9)-C(8)	118.4(3)	118.970	C(24)-C(23)-H(23)	121.7	121.741
C(10)-C(9)-H(9)	120.8	120.827	N(6)-C(24)-C(19)	105.6(3)	104.784
C(8)-C(9)-H(9)	120.8	120.193	N(6)-C(24)-C(23)	132.1(4)	132.592
C(11)-C(10)-C(9)	118.9(3)	118.320	C(19)-C(24)-C(23)	122.4(4)	122.624
C(11)-C(10)-H(10)	120.5	120.562	O(1)-S(1)-C(26)	105.8(3)	107.623
C(9)-C(10)-H(10)	120.5	121.112	O(1)-S(1)-C(25)	105.8(2)	107.188
N(3)-C(11)-C(10)	123.6(3)	123.309	C(26)-S(1)-C(25)	100.5(3)	97.462
N(3)-C(11)-H(11)	118.2	116.175	S(1)-C(25)-H(25A)	109.5	107.253
C(10)-C(11)-H(11)	118.2	120.513	S(1)-C(25)-H(25B)	109.5	109.180
N(3)-C(12)-C(8)	122.3(3)	122.752	H(25A)-C(25)-H(25B)	109.5	109.499
N(3)-C(12)-C(13)	113.1(3)	113.394	S(1)-C(25)-H(25C)	109.5	110.137
C(8)-C(12)-C(13)	124.3(3)	123.720	H(25A)-C(25)-H(25C)	109.5	110.110
N(4)-C(13)-C(14)	120.6(3)	120.776	H(25B)-C(25)-H(25C)	109.5	109.499
N(4)-C(13)-C(12)	120.4(3)	119.845	S(1)-C(26)-H(26A)	109.5	109.173
C(14)-C(13)-C(12)	118.8(3)	119.207	S(1)-C(26)-H(26B)	109.5	109.892
C(15)-C(14)-C(13)	118.9(3)	118.988	H(26A)-C(26)-H(26B)	109.5	111.402
C(15)-C(14)-C(18)	121.3(3)	120.381	S(1)-C(26)-H(26C)	109.5	107.036
C(13)-C(14)-C(18)	119.6(3)	120.612	H(26A)-C(26)-H(26C)	109.5	109.194
			H(26B)-C(26)-H(26C)	109.5	110.036

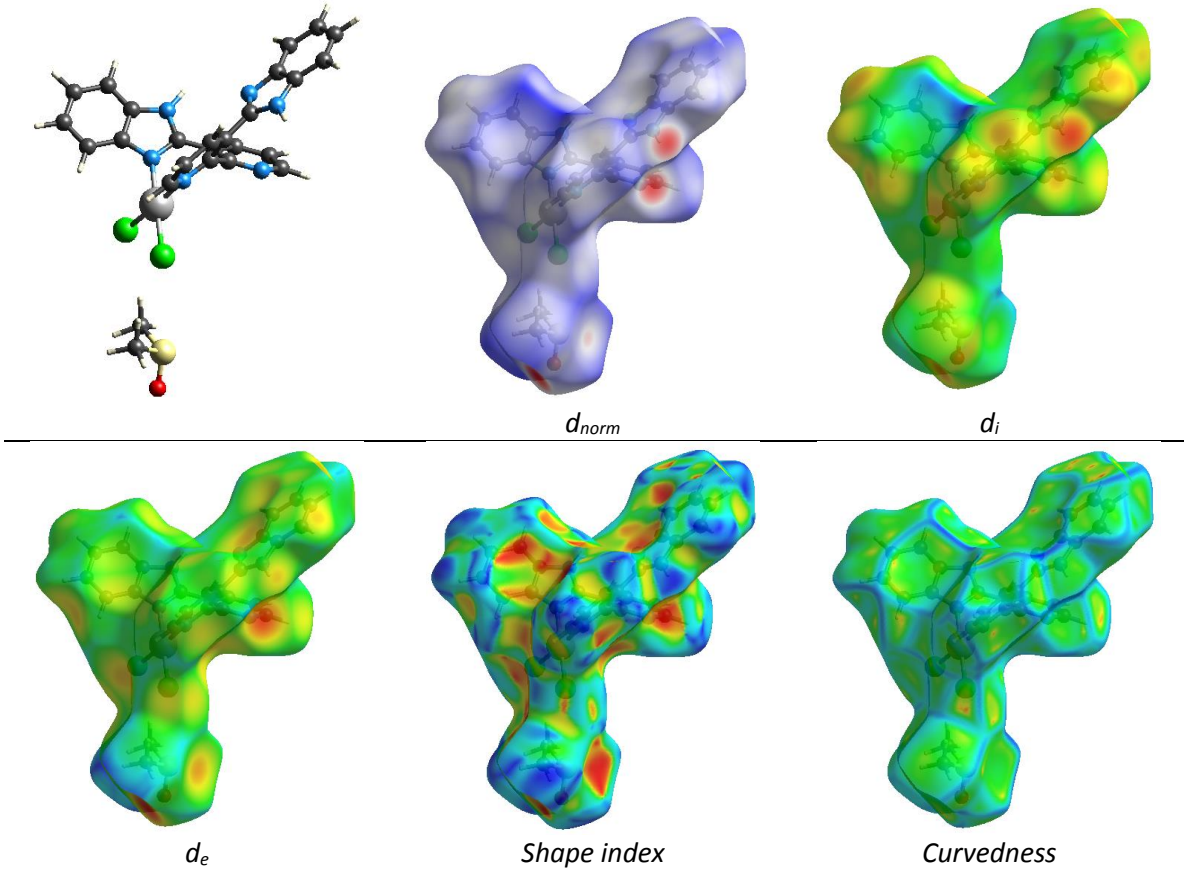

d_{norm} in the ranges -0.7499 to 1.6737 *a.u.;* d_i in the ranges -0.6435 to 3.1332 Å; d_e in the ranges -0.6456 to 2.9454 Å; *Shape index* in the ranges -1.0000 to 1.0000 *a.u.; Curvedness* in the ranges -4.0000 to 0.4000 *a.u.*

Fig. S4. Hirsfeld surface mapped with d_e, d_i, d_{norm}, shape index, and curvedness of **1**

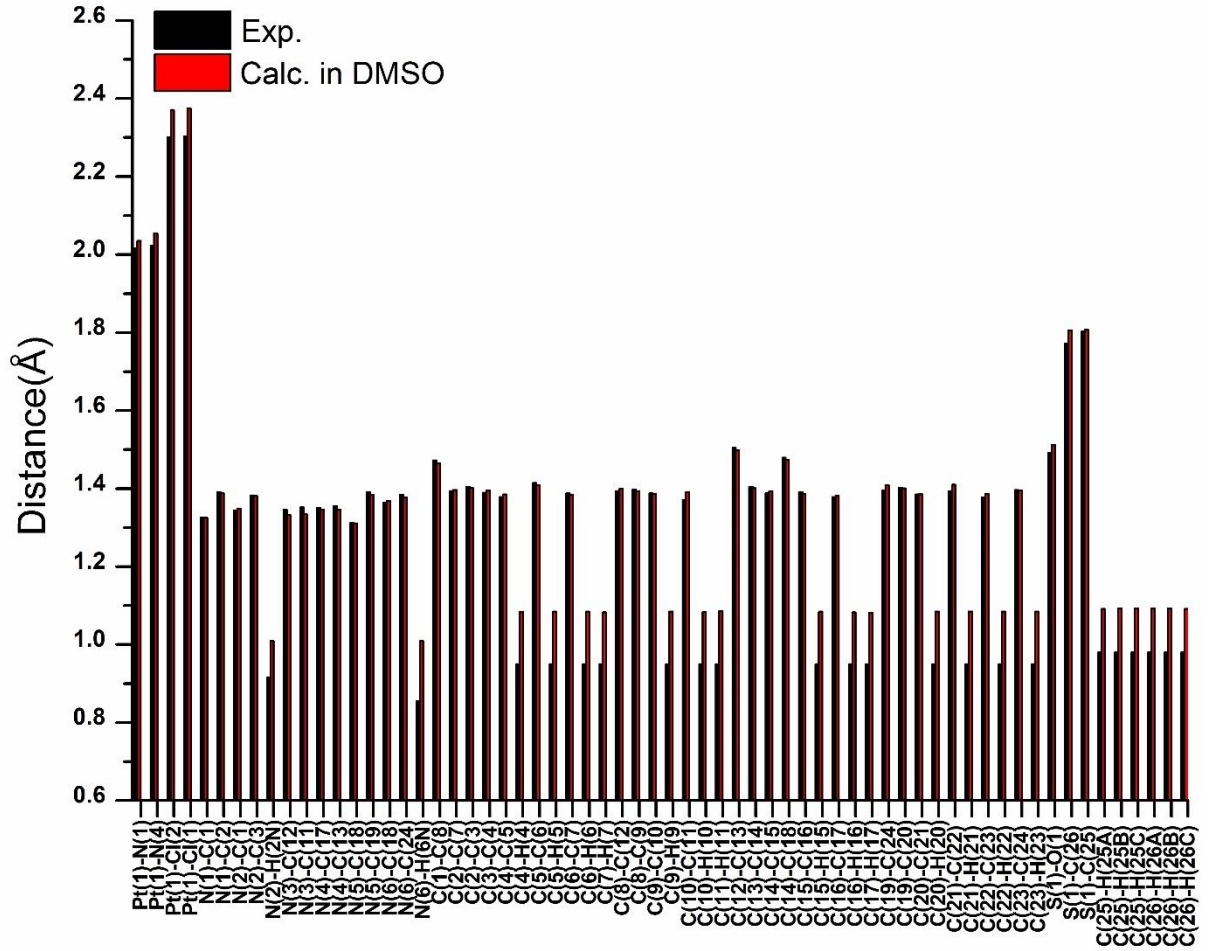

Fig. S5. Experimental and calculated bond lengths for **1**

Table S3. Dipole moments (μ, Debye), the sum of electronic energies including zero-point energy corrections (E_{elec}+ZPE), the sum of electronic energies including thermal free energies (E_{elec}+ΔG) for the investigated compounds, and stabilization energies at 0 K (ΔE) and room temperature (ΔΔG) for the dimer formation in DMSO

	1	Dimer
μ (D)	22.86	36.02
E_{elec} + ZPE (Hartree)	-2844.7058	-5689.4905
E_{elec}+ΔG (Hartree)	-2844.7744	-5689.6007
ΔE (kcal/mol)	-	-49.55
ΔΔG (kcal/mol)	-	-32.63

$\Delta E = [(E+ZPE)_{Dimer} - 2x(E+ZPE)_{Monomer(1)}]$; $\Delta\Delta G = [(\Delta G +ZPE)_{Dimer} - 2x(\Delta G +ZPE)_{Monomer(1)}]$

Table S4. NBO charges for monomer and dimer at ωB97XD/6-31G(d,p)/LANL2DZ in DMSO

Monomer		Dimer		Monomer		Dimer		Dimer		Dimer	
Atom No	Charge	Atom No	Charge	Atom No	Charge	Atom No	Charge	Atom No	Charge	Atom No	Charge
Pt1	0.363	Pt1	0.376	C15	-0.149	C 31	-0.160	Pt 50	0.375	H 81	0.282
Cl1	-0.508	Cl2	-0.520	H(15C)	0.232	H 32	0.282	Cl 51	-0.519	C 82	-0.255
Cl2	-0.497	Cl3	-0.503	C16	-0.254	C 33	-0.255	Cl 52	-0.503	H 83	0.294
N1	-0.482	N4	-0.480	H(16C)	0.288	H 34	0.294	N 53	-0.482	C 84	0.068
N2	-0.539	N5	-0.553	C17	0.065	C 35	0.069	N 54	-0.552	H 85	0.276
N3	-0.461	N6	-0.499	H(17C)	0.261	H 36	0.277	N 55	-0.502	C 86	0.409
N4	-0.428	N7	-0.424	C18	0.419	C 37	0.409	N 56	-0.424	C 87	0.105
N5	-0.524	N8	-0.536	C19	0.103	C 38	0.107	N 57	-0.535	C 88	-0.250
N6	-0.570	N9	-0.578	C20	-0.246	C 39	-0.252	N 58	-0.578	H 89	0.257
C1	0.484	C10	0.471	H(20C)	0.261	H 40	0.256	C 59	0.473	C 90	-0.263
C2	0.134	C11	0.133	C21	-0.268	C 41	-0.262	C 60	0.134	H 91	0.255
C3	0.137	C12	0.134	H(21C)	0.257	H 42	0.255	C 61	0.134	C 92	-0.242
C4	-0.259	C13	-0.260	C22	-0.251	C 43	-0.241	C 62	-0.260	H 93	0.256
H(4C)	0.274	H14	0.272	H(22C)	0.258	H 44	0.256	H 63	0.269	C 94	-0.263
C5	-0.240	C15	-0.246	C23	-0.272	C 45	-0.264	C 64	-0.246	H 95	0.257
H(5C)	0.265	H16	0.262	H(23C)	0.265	H 46	0.257	H 65	0.262	C 96	0.133
C6	-0.249	C17	-0.253	C24	0.127	C 47	0.133	C 66	-0.253	H 97	0.469
H(6C)	0.265	H18	0.262	H(6N)	0.476	H48(9N)	0.469	H 67	0.262	H 98	0.489
C7	-0.244	C19	-0.245	H(2N)	0.490	H49 (5N)	0.485	C 68	-0.245	S 99	1.281
H(7C)	0.265	H20	0.270	S1	1.278	S 109	1.293	H 69	0.270	**O 100**	**-1.022**
C8	-0.127	C21	-0.115	O1	-1.023	O 110	-1.025	C 70	-0.112	C 101	-0.915
C9	-0.164	C22	-0.153	C25	-0.924	C 111	-0.921	C 71	-0.153	H 102	0.281
H(9C)	0.279	H23	0.282	H(25C)	0.260	H 112	0.263	H 72	0.281	H 103	0.279
C10	-0.267	C24	-0.262	H(25C)	0.275	H 113	0.282	C 73	-0.261	H 104	0.269
H(10C)	0.277	H25	0.280	H(25C)	0.265	H 114	0.279	H 74	0.281	C 105	-0.920
C11	0.044	C26	0.047	C26	-0.925	C 115	-0.921	C 75	0.045	H 106	0.263
H(11C)	0.253	H27	0.253	H(26C)	0.260	H 116	0.278	H 76	0.253	H 107	0.277
C12	0.224	C28	0.242	H(26C)	0.275	H 117	0.268	C 77	0.243	H 108	0.283
C13	0.266	C29	0.249	H(26C)	0.276	H 118	0.280	C 78	0.251		
C14	-0.094	C30	-0.100					C 79	-0.098		
								C 80	-0.161		

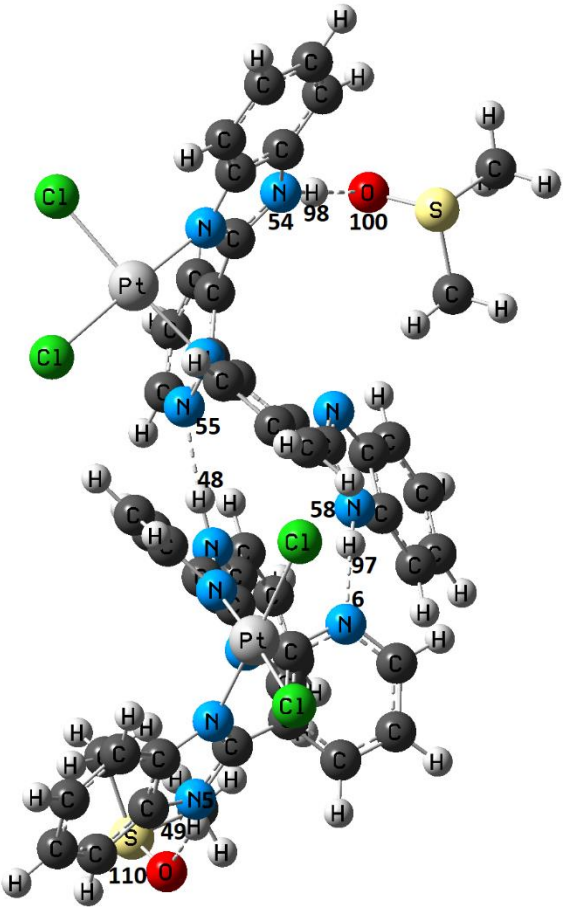

Fig. S6. Presentation of H-bonds and atom numbers for the dimer

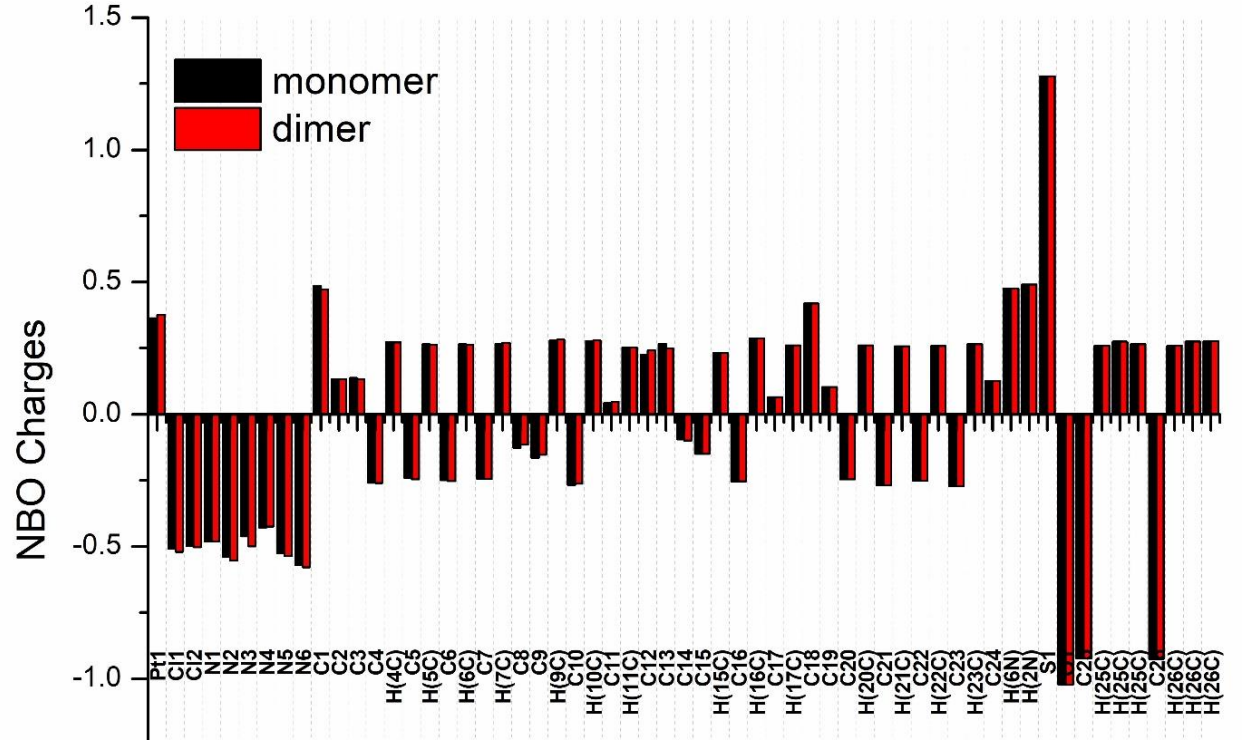

Fig. S7. NBO charges for monomer and the dimer at ωB97XD/6-31G(d,p)/LANL2DZ in DMSO

Table S5. Second-order perturbation theory analysis of Fock matrix on NBO basis for the dimer molecules by using the ωB97XD method with 6-31G(d,p)/LANL2DZ basis sets.

Donor (i)	Occupancy	Acceptor (j)	Occupancy	E(2)[a] kcal/mol	E(j)-E(i)[b] a.u.	F(i,j)[c] a.u.
LP[d] (N55)	1.888	σ* (N9-H48)	0.059	24.63	1.01	0.142
LP (N6)	1.890	σ* (N58-H97)	0.058	23.19	1.01	0.138
LP1 (O100)	1.882	σ* (N54-H98)	0.089	8.16	1.33	0.095
LP2 (O100)	1.882	σ* (N54-H98)	0.089	18.12	0.94	0.117
LP3 (O100)	1.846	σ* (N54-H98)	0.089	30.01	0.93	0.151
LP1 (O110)	1.965	σ* (N5-H49)	0.086	13.12	1.37	0.121
LP2 (O110)	1.892	σ* (N5-H49)	0.086	17.49	0.92	0.114
LP3 (O110)	1.850	σ* (N5-H49)	0.086	18.39	0.91	0.117

a: stabilization energy (energy of hyperconjugative interactions); b: Energy difference between donor and acceptor i and j NBO orbitals; c: Fock matrix element between i and j NBO orbitals
d: valence lone pair electron on O and N atom; E(2) = qi [$(F(i,j)^2)$/E(j)-E(i)] equation defines stabilization energy related to second order perturbation theory.

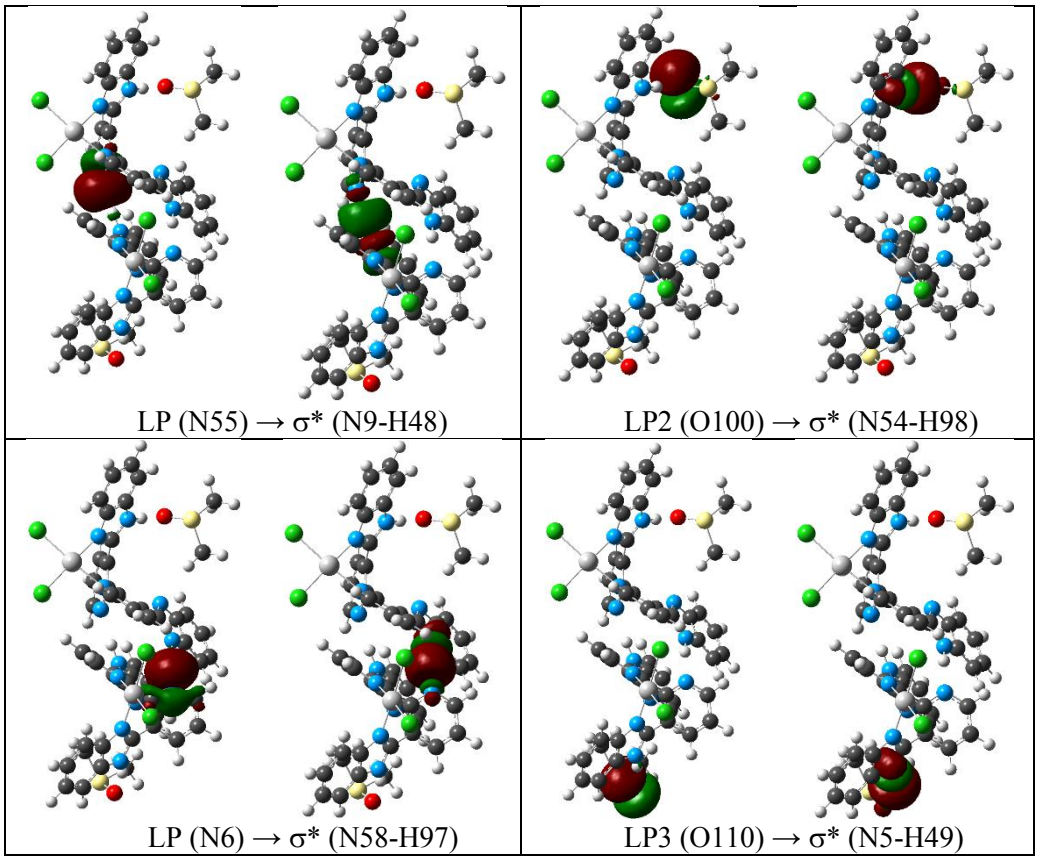

Fig. S8. Molecular orbitals involved in the H-bond formation

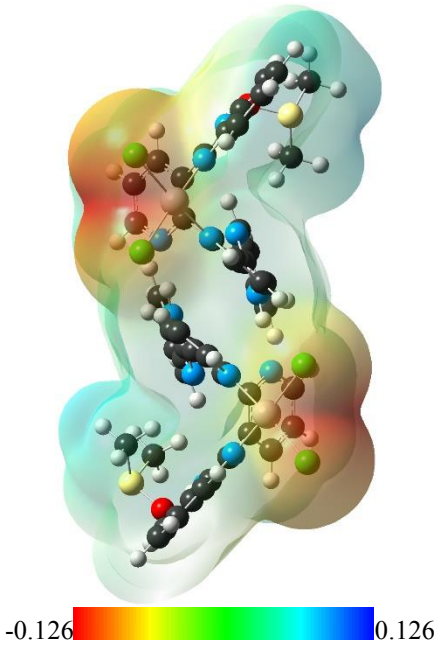

Fig. S9. Molecular electrostatic potential surface map for the dimer compound in DMSO calculated at wB97XD/6-31G(d,p)/LANL2DZ level (isovalue is 0.02 a.u.). Colours represent electron density: red, electron-rich; yellow, slightly electron-rich region; green, neutral; light blue, slight electron deficiency; blue, electron deficiency.

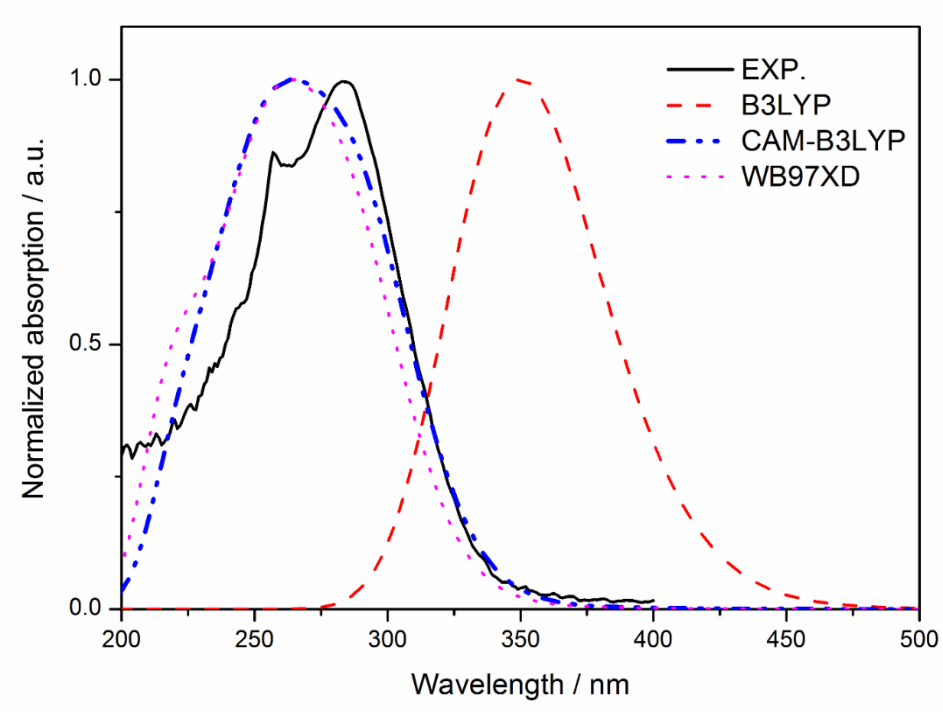

Fig. S10. Experimental and calculated (with different functionals) normalized UV-Vis absorption spectra for the dimer in DMSO

Table S6. Electronic transitions (λ_{ex}) corresponding to vertical excitation energies (ΔE), oscillator strengths (f), excitation character, molecular orbitals, and their % contributions of dimer in DMSO calculated with TD-DFT at CAM-B3LYP/6-31G(d,p)/LANL2DZ levels

state	ΔE (eV)	λ_{ex} (nm)	f	Character[a]	Predominant Transitions	%
S_1	3.209	386.3	0.0012	d-d,LE2	H-8→L+6	30
				d-d,LE2	H-9→L+6	29
S_2	3.212	386.0	0.0012	d-d,LE2	H-9→L+7	31
				d-d,LE2	H-8→L+6	17
S_3	3.46	358.3	0.0010	LMCT1,d-d	H-2→L+6	31
				LMCT1,d-d	H-17→L+6	27
S_4	3.48	356.6	0.0015	MLCT1,d-d	H-4→L+7	37
S_5	3.55	348.9	0.0026	d-d,LE2	H-11→L+6	39
S_6	3.56	348.3	0.0026	d-d,LE2	H-10→L+7	39
S_7	3.71	334.5	0.0018	d-d,LE2	H-12→L+6	33
S_9	4.09	303.3	0.0873	CT1	H→L	54
S_{10}	4.23	293.1	1.2694	CT1	H→L+3	50
S_{11}	4.41	281.1	0.2081	CT2	H→L+2	44
S_{12}	4.42	280.7	0.1792	CT2	H→L+1	55
S_{13}	4.58	270.4	0.0092	MLCT1	H-9→L+1	27
S_{15}	4.63	267.7	0.0507	CT1	H-1→L	44
S_{16}	4.67	265.2	0.2381	CT1	H-1→L+3	25
S_{17}	4.69	264.5	0.2517	MLCT2,LE3	H-4→L+4	24
S_{19}	4.75	260.8	0.0927	CT2	H-2→L+1	28
S_{21}	4.91	252.7	0.0552	CT2	H-4→L	22
S_{22}	4.91	252.4	0.1176	CT4	H→L+5	21
				MLCT3	H-6→L+5	18
S_{24}	4.95	250.6	0.1097	MLCT2	H-11→L+2	20
				MLCT2	H-9→L	19
S_{25}	4.97	249.4	0.1128	CT2	H-1→L+2	28
				CT1	H-1→L	24
S_{27}	4.99	248.5	0.1046	CT2	H-1→L+1	40
S_{30}	5.02	246.9	0.2344	MLCT4	H-9→L+4	16
				CT5	H→L+4	15

[a]LE1: local excitation of Pt,d-d; LE2: local excitation Cl atoms; LE3: local excitation bim; MLCT1: charge transfer from Pt to py2 and py2'; MLCT2: charge transfer from Pt, Cl to py1 and py2; MLCT3: charge transfer from Pt, Cl to py1; MLCT4: charge transfer from Pt, Cl to py1 and bim1; LMCT1: charge transfer from bim1' to Pt; CT1: charge transfer from bim2 to py2; CT2: charge transfer from bim2 to py1 and py2; CT3: charge transfer from bim1' to py2; CT4: charge transfer from bim2 to py1', py2' and bim1'; CT5: charge transfer from bim2 to py1 and bim1. H: HOMO, L: LUMO

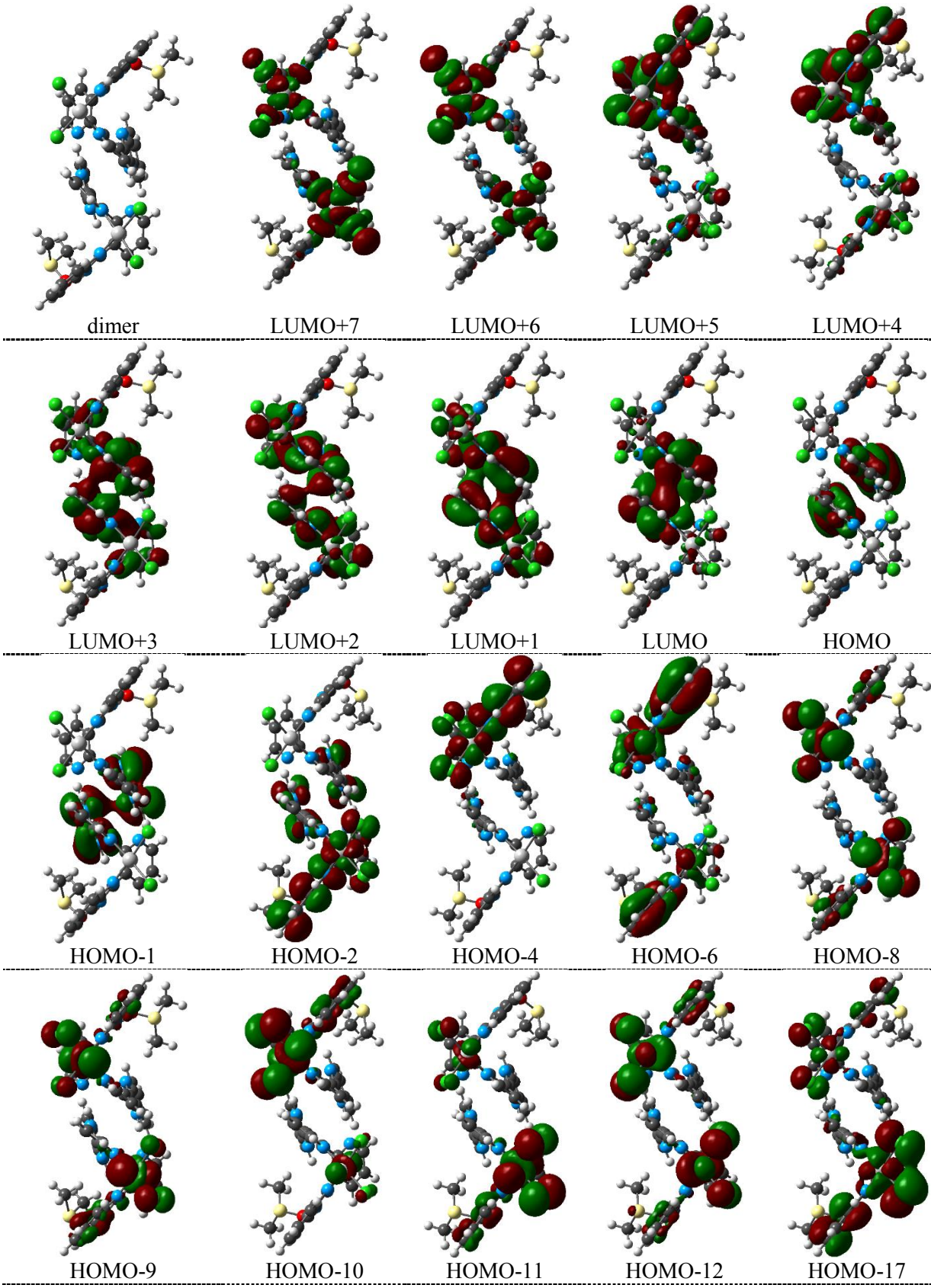

Fig. S11. Selected molecular orbitals of dimer in DMSO at CAM-B3LYP/6-31G(d,p)/LANL2DZ levels (isovalue is 0.02 a.u.)

Conflicts of Interest: The authors declare no conflict of interest